Natural Convective Flow Instability Between Horizontal Concentric Cylinders

D. B. Fant*
Air Force Office of Scientific Research, Washington, D.C. 20332
and
A. Rothmayer† and J. Prusa‡
Iowa State University, Ames, Iowa 50011

Thermal and hydrodynamic instabilities are numerically investigated for natural convective flow between narrow horizontal cylindrical annuli. At fairly high Rayleigh numbers, thermal instability for air appears as steady, counter-rotating cells near the top portion of the annulus. This flow also yields hysteresis behavior under certain small gap width conditions. For small Prandtl number fluids, an unsteady hydrodynamic instability is demonstrated at high Grashof numbers in the vertical portions of narrow annuli. These cells are like-rotating. For the high Rayleigh number, small gap width regime, excellent agreement is achieved between an existing analytical boundary-layer result and present Navier-Stokes computations.

Introduction

FROM a practical standpoint, the study of natural convection between horizontal isothermal concentric cylinders has a wide variety of technological applications, ranging from nuclear reactors and thermal storage systems to cooling of electronic components, aircraft fuselage insulation, underground electrical transmission lines, and even the flow in the cooling passages of turbine blades.[1]

However, in a different perspective, the work set forth in this research was undertaken to gain further understanding of natural convective flow instabilities in a two-dimensional geometry. Still not well understood is the influence of Prandtl number Pr variations on the nonlinear processes involved in triggering either thermal or hydrodynamic types of instability. Also of relevance is the aspect of nonuniqueness, which allows the possibility of hysteresis behavior associated with thermal-convective instabilities. These important issues are addressed and studied in this paper.

For horizontal isothermal concentric cylinders, the basic flowfield consists of two cresent shaped cells induced strictly from buoyancy effects, although more complicated flowfields can develop, depending on the Rayleigh number and diameter ratio R considered. For air, Powe et al.[2] experimentally characterized three basic flow regimes associated with the top portion of an annulus: 1) two-dimensional multicellular flow for $R \leq 1.2$, 2) three-dimensional spiral flow for $1.2 < R \leq 1.7$, and 3) three-dimensional oscillatory flow for $R > 1.7$. The counter-rotating multicellular flowfield in regime 1 remained steady for a small number of cells, but as Rayleigh number increased, slight oscillations about the vertical centerline occurred. Regimes 2 and 3 are unsteady.

Other studies relating to this can be found in Liu et al.,[3] Grigull and Hauf,[4] Bishop et al.,[5] Powe et al.,[6] Kuehn and Goldstein,[7] and Rao et al.[8] A collective review of these articles is given in Fant.[9]

In general, experimenters have verified that, for air at high Rayleigh numbers, a two-dimensional multicellular flow is possible near the top of narrow horizontal cylindrical annuli. However, not all numerical investigations have confirmed this fact. It seemed that the transition to multicells could not be captured due to either first-order upwind differencing of the convective terms or a lack of numerical stability experienced when approaching high Rayleigh numbers. Thus, it appears that at least second-order accuracy is required to resolve this multicellular type of instability. In addition, for this geometry, there appears to be a void in the research regarding the possibility of related hysteresis behavior associated with the transition to multicells. The lack of numerical results in this area provided motivation for the thermal instability work reported in this paper.

For small Prandtl numbers, an apparent thermal-like instability was resolved analytically by Mack and Bishop[10] for a relatively wide annular gap of diameter ratio 2.0 (also see Huetz and Petit[11]). This two-dimensional steady flow consisted of six counter-rotating cells in the full annulus. A similar type of instability was also reported by Fant[9] for $Pr = 0.02$ and $R = 2.0$.

Interestingly, in this study, for vanishingly small Prandtl numbers and $R = 1.09$ (a narrow gap width), an unsteady multicellular flow with like-rotating cells was resolved numerically in the vertical portion of the annulus. This instability is hydrodynamic in nature and is qualitatively similar to that investigated by Elder[12] and Lee and Korpela[13] for a narrow vertical slot geometry; although, for the vertical slot, the multicellular flow remained steady for small Prandtl number fluids.

Fant et al.[14] appear to have been the first to identify this type of two-dimensional, unsteady, hydrodynamic instability in the vertical portion of a narrow horizontal cylindrical annulus. However, their results related to the numerical solution of boundary-layer-like equations, obtained by simplifying the two-dimensional Navier-Stokes equations under the limits of small Prandtl number, high Rayleigh number, and small gap width. The current study relaxes two of these important constraints by solving the two-dimensional Navier-Stokes equations for the single limiting condition of small Prandtl number. Qualitative and quantitative comparisons appear later in the paper.

This particular multicellular flow instability has only been captured numerically, as previously discussed, whereas the analogous instability for the vertical slot geometry has been studied and verified both experimentally and numerically.

Because of the lack of numerical and experimental work associated with the low Prandtl number regime, further im-

Received Dec. 18, 1989; revision received June 27, 1990; accepted for publication Aug. 6, 1990. This paper is declared a work of the U.S. Government and is not subject to copyright protection in the United States.

*Program Manager.
†Associate Professor.
‡Associate Professor.

petus was provided to study this unique flow in more detail in the present paper. Thus, the narrow gap annular geometry offers the capability of examining both thermal and hydrodynamic instabilities, dictated by the Prandtl number of the working fluid.

Mathematical Analysis

The basic mathematical formulation is as given in Fant et al.[14] The flow is assumed to be laminar, Newtonian, and two dimensional, and the inner cylinder temperature is assumed to exceed the outer. The geometry for this problem is shown in Fig. 1. Also, the vorticity stream function formulation of the Navier-Stokes equations is adopted. Cast in dimensionless form, the governing equations are the following:

Energy:

$$G^2\frac{\partial T}{\partial t} + Gu\frac{\partial T}{\partial r} + \frac{Gv}{R + G^{-1}}\frac{\partial T}{\partial \psi} = Pr^{-1}\left[\frac{\partial^2 T}{\partial r^2} + \frac{1}{r + G^{-1}}\frac{\partial T}{\partial r} + \frac{1}{(r + G^{-1})^2}\frac{\partial^2 T}{\partial \psi^2}\right] \quad (1)$$

Vorticity:

$$Pr\left\{G^2\frac{\partial w}{\partial t} + Gu\frac{\partial w}{\partial r} + \frac{Gv}{r + G^{-1}}\frac{\partial w}{\partial \psi}\right\} = Pr\left[\frac{\partial^2 w}{\partial r^2} + \frac{1}{r + G^{-1}}\frac{\partial w}{\partial r} + \frac{1}{(r + G^{-1})^2}\frac{\partial^2 w}{\partial \psi^2}\right] + G\,Ra\left(\sin\psi\frac{\partial T}{\partial r} + \frac{\cos\psi}{r + G^{-1}}\frac{\partial T}{\partial \psi}\right) \quad (2)$$

Stream function:

$$\frac{\partial^2 f}{\partial r^2} + \frac{1}{r + G^{-1}}\frac{\partial f}{\partial r} + \frac{1}{(r + G^{-1})^2}\frac{\partial^2 f}{\partial \psi^2} = G^2 w \quad (3)$$

In these equations, u is the radial velocity, v the azimuthal velocity, f the stream function, w the vorticity, and T the temperature. The stream function is given by

$$u = \frac{-1}{G(r + 1/G)}\frac{\partial f}{\partial \psi} \quad (4a)$$

$$v = \frac{1}{G}\frac{\partial f}{\partial r} \quad (4b)$$

The radial and azimuthal coordinates r and ψ are shown in Fig. 1, and t is time. In this system of equations, three independent parameters are needed to describe the problem, namely, the Rayleigh number, the Prandtl number, and the gap spacing. The Rayleigh number is based on the temperature difference between the cylinders and the inner cylinder radius:

$$Ra = \frac{g\beta\, a^3(T_i - T_o)}{\nu\alpha} \quad (5)$$

where g is the local uniform vertical acceleration due to gravity, β the coefficient of thermal expansion, a the inner cylinder radius, ν the kinematic viscosity of the fluid, and α the thermal diffusivity. T_i and T_o are the inner and outer cylinder temperatures, respectively (see Fig. 1). The Prandtl number is given by

$$Pr = \frac{\nu}{\alpha} \quad (6)$$

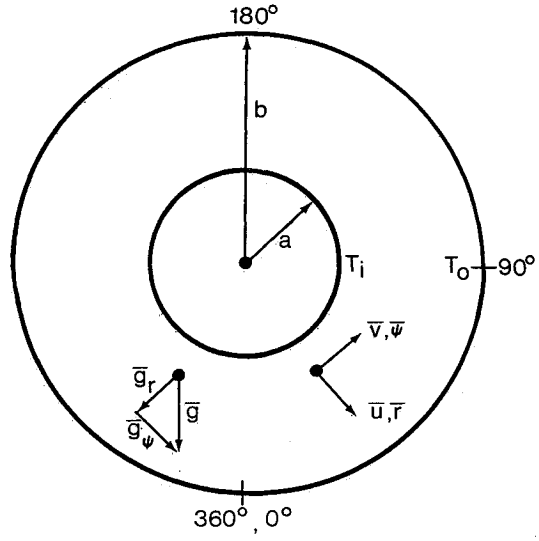

Fig. 1 Two-dimensional concentric cylinder geometry.

Finally, the gap spacing of the annulus is

$$G = \frac{b - a}{a} \quad (7)$$

where a is the radius of the inner cylinder and b is the radius of the outer cylinder. The time, the angular coordinate, and the radial coordinate have been nondimensionalized, as in Prusa and Yao.[15]

The nondimensional boundary conditions for this system of equations are the following:

The $r = 0$ (inner cylinder) boundary conditions:

$$T(\psi, 0) = 1 \quad (8)$$

$$f(\psi, 0) = 0 \quad (9)$$

$$w(\psi, 0) = G^{-2} f_{rr}(\psi, 0) \quad (10)$$

Similar boundary conditions are applied to the outer cylinder:

$$T(\psi, 1) = 0 \quad (11)$$

$$f(\psi, 1) = 0 \quad (12)$$

$$w(\psi, 1) = G^{-2} f_{rr}(\psi, 1) \quad (13)$$

Eqs. (1–3) will be used to examine the thermal instability of air for the concentric cylinder geometry. For the hydrodynamic instability analysis, small Prandtl number limiting equations will be derived next.

Small Prandtl Number Equations

In the limit $Pr \to 0$, the thermal-energy equation becomes

$$\frac{\partial^2 T}{\partial r^2} + \frac{1}{r + G^{-1}}\frac{\partial T}{\partial r} + \frac{1}{(r + G^{-1})^2}\frac{\partial^2 T}{\partial \psi^2} = 0 \quad (14)$$

subject to the following boundary conditions (assuming symmetry):

$$T(0, \psi) = 1 \quad (15a)$$

$$T(1, \psi) = 0 \quad (15b)$$

$$\frac{\partial T}{\partial \psi}(r, \psi = 0, \pi) = 0 \quad (15c)$$

Given Eqs. (15a–c), the solution to Eq. (14) is

$$T = 1 - \frac{\ell n(1 + G \cdot r)}{\ell n(1 + G)} \tag{16}$$

which is simply the steady-state conduction solution for the concentric cylindrical annulus. Because Eq. (16) is independent of ψ, one gets

$$\frac{\partial T}{\partial \psi} = 0 \tag{17a}$$

$$\frac{\partial T}{\partial r} = \frac{-G}{(1 + G \cdot r)\ \ell n(1 + G)} \tag{17b}$$

Hence, for the limit $Pr \to 0$, the buoyancy term $\sim \cos \psi\ (\partial T/\partial \psi)$ in Eq. (2) reduces to zero, whereas

$$\sin \psi \frac{\partial T}{\partial r} = \frac{-G \sin \psi}{(1 + G \cdot r)\ \ell n(1 + G)} \tag{18}$$

Thus, the energy equation has decoupled itself from the vorticity equation.

Now, in the limit $G \to \infty$, Eq. (18) vanishes (or approaches zero from the negative side). As $G \to 0$, Eq. (18) simplifies to

$$\sin \psi \frac{\partial T}{\partial r}\bigg|_{G \to 0} = -\sin \psi \tag{19}$$

Therefore, $\sin \psi(\partial T/\partial r)$ achieves its maximum absolute value (and thus maximum velocity) at $\psi = 90$ and 270 deg for $G \to 0$. This indicates that for the $Pr \to 0$ condition, a hydrodynamic (or shear-flow) instability will likely occur in the vertical portions of a narrow annulus.

Incorporating these simplifications, the governing equations for the $Pr \to 0$ limit become the following:

Vorticity:

$$G^2 \frac{\partial w}{\partial t} + \left(r + \frac{1}{G}\right)^{-1} \left(\frac{\partial f}{\partial r}\frac{\partial w}{\partial \psi} - \frac{\partial f}{\partial \psi}\frac{\partial w}{\partial r}\right) = \frac{\partial^2 w}{\partial r^2} + \frac{1}{r + G^{-1}}\frac{\partial w}{\partial r} + \frac{1}{(r + G^{-1})^2}\frac{\partial^2 w}{\partial \psi^2} + G(Gr)\left[\frac{-G \sin \psi}{(1 + G \cdot r)\ \ell n(1 + G)}\right] \tag{20}$$

Stream function:

$$\frac{\partial^2 f}{\partial r^2} + \frac{1}{r + G^{-1}}\frac{\partial f}{\partial r} + \frac{1}{(r + G^{-1})^2}\frac{\partial^2 f}{\partial \psi^2} = G^2 w \tag{21}$$

With boundary conditions:

$$f(0, \psi) = f(1, \psi) = 0 \tag{22}$$

$$w(r = 0, 1; \psi) = \frac{1}{G^2}\frac{\partial^2 f}{\partial r^2}\bigg|_{r=0,1} \tag{23}$$

As seen by Eqs. (20) and (21), the nonlinear terms in the vorticity (momentum) equation remain and the energy equation decouples and reduces to the simple conduction solution. Most important, though, these small Pr equations are valid for arbitrary gap width G and Grashof number Gr, thus enabling one to further investigate the various effects of each parameter.

Analytical Solutions

A steady-state analytical solution to Eqs. (1–3) was derived in Fant.[9] This solution was obtained by considering the Navier-Stokes equations under the limiting conditions of high Rayleigh number and small gap width. The resultant asymptotic expansions for temperature, vorticity, and stream function are the following:

$$\tilde{T} = (1 - r) + \tilde{G}^4 T_1 + \tilde{G}^8 T_2 + \tilde{G}^{12} T_3 + \mathcal{O}(\tilde{G}^{16}) \tag{24}$$

$$\tilde{w} = \tilde{G} w_1 + \tilde{G}^5 w_2 + \tilde{G}^9 w_3 + \tilde{G}^{13} w_4 + \mathcal{O}(\tilde{G}^{17}) \tag{25}$$

$$\tilde{f} = \tilde{G}^3 f_1 + \tilde{G}^7 f_2 + \tilde{G}^{11} f_3 + \tilde{G}^{15} f_4 + \mathcal{O}(\tilde{G}^{19}) \tag{26}$$

where

$$T_1 = \frac{\cos \psi}{1440}[r(2r^5 - 6r^4 + 5r^3 - 1)] \tag{27}$$

$$w_1 = \frac{\sin \psi}{2\ Pr}\left[r(r - 1) + \frac{1}{6}\right] \tag{28}$$

$$f_1 = \frac{\sin \psi}{24\ Pr}[r^2(r - 1)^2] \tag{29}$$

As shown in Fant,[9] these expansions were based on the scaling,

$$(w, f, T) \sim (Ra^{3/4}\ \tilde{w}, Ra^{1/4}\ \tilde{f}, \tilde{T}) + \cdots \tag{30}$$

Also, higher order terms for Eqs. (24–26) may be found in this reference. In these equations, $\tilde{G}$ is defined as

$$\tilde{G} = Ra^{1/4}\ G \tag{31}$$

Similar results were obtained for the small Prandtl number limiting condition of the above equations. For this case, the dependent variables expand as

$$T = 1 - r \tag{32}$$

$$W = \hat{G}\ W_1 + \hat{G}^5\ W_2 + \mathcal{O}(\hat{G}^9) \tag{33}$$

$$F = \hat{G}^3\ F_1 + \hat{G}^7\ F_2 + \mathcal{O}(\hat{G}^{11}) \tag{34}$$

where

$$W_1 = \frac{[r^2 - r + (1/6)] \sin \psi}{2} \tag{35}$$

$$F_1 = \frac{r^2(r - 1)^2 \sin \psi}{24} \tag{36}$$

Notice that a new scaled gap $\hat{G}$ is defined such that

$$\hat{G} = Gr^{1/4}\ G \tag{37}$$

These expansions were based on the following scaling:

$$(\tilde{w}, \tilde{f}, \tilde{T}) \sim (Pr^{-3/4}\ W, Pr^{-1/4}\ F, T) + \cdots \tag{38}$$

The preceding analytical solutions, valid for finite and vanishingly small Prandtl numbers, will provide useful comparisons to the numerical results appearing later in the paper.

Computational Method

The two-dimensional Navier-Stokes equations, Eqs. (1–3) and the small Prandtl number Navier-Stokes equations, Eqs. (20) and (21), were solved implicitly in time using a point-

iterative Gauss-Seidel procedure with under-relaxation. The dependent variables at a given time level were found by repeated iteration of the governing equations until a local relative error of $1/10^6$ was achieved. The solutions were carried out to steady state whenever possible, and when unsteady flow behavior occurred, sufficiently small time steps were used to avoid large truncation errors and produce time-accurate solutions.

For the unsteady terms, a first-order forward difference formula was employed. All spatial derivatives in the governing equations were second order centrally differenced. This included the radial and streamwise convective terms that were represented by a first-order upwind expression together with the standard correction term to give a second-order central difference form in the converged solution. Variable spatial increments were also used in order to concentrate nodes near the inner and outer cylinders and near multicellular activity.

The transitional value of Ra or Gr (that value that characterizes the transition from bicellular to multicellular flow) was determined by initially calculating the steady-state bicellular solutions for successively larger pretransitional values of Ra or Gr. Each successive steady-state calculation was run using the previously converged steady-state solution as an initial guess. This procedure was repeated until, at some critical value of Ra or Gr, a transition to multicellular flow occurred. The primary aim of this study was to numerically capture both thermal instability (transitional Ra for air) and hydrodynamic instability (transitional Gr for small Pr) in a narrow horizontal annulus. For the small Prandtl number solutions, unsteady periodic motion was determined. Note that, in these cases, each time level of the unsteady calculation was completely iterated to convergence.

For the small Prandtl number Navier-Stokes equations, symmetry about the vertical centerline was assumed for a 31 $\times$ 102 size mesh (31 radial nodes and 102 angular nodes). Finer meshes were also considered and will be discussed in the next section. Overall, though, the 31 $\times$ 102 mesh adequately resolved the multicells that formed within the annulus. This symmetry assumption was based on the work of Fant et al.[14] By considering the complete annulus, they verified the vertical symmetry condition for the numerical solution of small Prandtl number boundary-layer equations. This assumption was, therefore, extended to the small Prandtl number equations studied in this paper. In qualitative support of this claim, the multicells were concentrated near the vertical section of the annulus, whereas the flow near $\psi = 0$ and 180 deg remained quiescent, preserving the steady-state kidney-shaped flow pattern in these regions. Also, the small Prandtl number steady-state analytical solutions were symmetric about $\psi = 0$ and 180 deg.

For the thermal instability of air, calculations were based on a 31 $\times$ 102 mesh for the entire annulus ($0-2\pi$). Nodes were highly concentrated near the top of the annulus to properly resolve the counter-rotating secondary motion in this region. For the cases considered, steady-state symmetric solutions ensued.

The CPU time varied considerably depending on the multicellular activity that developed. For thermal instability, steady-state pretransitional solutions were achieved within 300 time steps for $\Delta t = 5 \times 10^{-4}$. This required a total CPU time of about 5 h on a Perkin-Elmer 3242, a supermini computer with a computing speed of about 1 MIP. However, when the transition to multicells occurred (two to four or two to six cells), the time step was maintained at 5×10^{-4}, but the amount of CPU time needed to achieve steady state increased to approximately 30 h.

The unsteady small Prandtl number results were calculated on the VAX 8650 computer system. For the unsteady multicellular flow corresponding to $Gr = 1.45 \times 10^6$ and $G = 0.09$, some 120 h of CPU time were required to compute this solution up to a dimensionless time of $t = 0.75$ for a constant time step of 5×10^{-5} (see Fig. 12).

Numerical Results and Discussion

The first part of this section describes the hysteresis behavior associated with steady multicellular flow occurring in narrow gaps for air. This type of multicellular flow is a result of thermal instability and develops near the top portions of narrow horizontal annuli.

The second section mainly describes an unsteady multicellular flow that develops near the vertical portions of a narrow horizontal annulus for small Prandtl number fluids. This particular type of instability is hydrodynamic in origin.

Thermal Instability

For the two-dimensional Navier-Stokes equations, multicellular flow near the top of the annulus was investigated for $Pr = 0.706$. The complete annular flowfield ($0-2\pi$) was determined numerically when searching for hysteresis behavior. A 31 $\times$ 102 mesh was employed with the grid points concentrated near the top horizontal portion of the annulus where the multicellular flowfield tended to develop for air.

Average Nusselt numbers are presented in Fig. 2 for gap number $G = 0.200$ and $Pr = 0.706$. The transition of the flowfield from two to four cells occurred abruptly at a Rayleigh number of approximately 3.51×10^5 (or 2808, when based on gap width). Associated with this transition was a sudden rise in the average Nusselt number (see Fig. 2) due mainly to more efficient fluid mixing created by the counter-rotating secondary motion.

The Nusselt number exhibited a hysteresis behavior as the Rayleigh number was gradually increased and then decreased past the transition point. For $Ra > 3.5 \times 10^5$, only a four-cell solution prevailed; whereas for $Ra < 2.85 \times 10^5$, only a two-cell solution prevailed. However, between these two limits, both types of solutions were possible, thus forming a hysteresis loop.

Powe et al.[6] numerically estimated a transitional Rayleigh number of 4.52×10^5 for $G = 0.200$, based on the point at which the stream function changed its sign. However, they could not fully resolve the smaller counter-rotating cell with their particular method. They used a uniform increment mesh with 35 angular and 15 radial nodes for the half-annulus. A similar four-cell flow pattern was experimentally observed by Bishop et al.[16] in a concentric spherical geometry. For $G = 0.19$, they obtained a transitional Rayleigh number (based on gap width) of about 3.6×10^3, which corresponds to approximately $Ra = 5.25 \times 10^5$.

These earlier results agree with the present work in that a four-cell pattern predominates immediately after the thermal instability sets in for $G = 0.200$.

Streamline plots of the cellular flowfield for $G = 0.200$ are depicted in Figs. 3 and 4. Figure 3 corresponds to $Ra = 3.5 \times 10^5$ and demonstrates the usual kidney-shaped flow pattern.

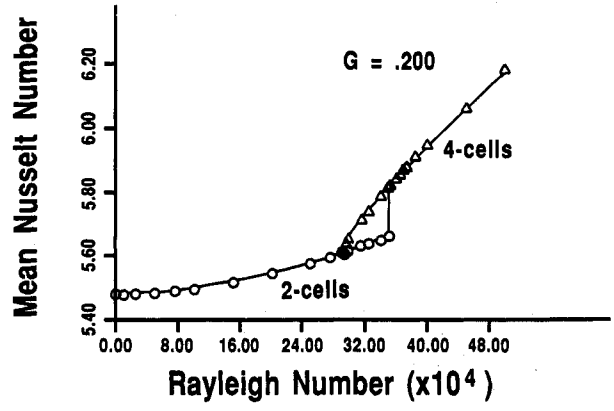

Fig. 2 Hysteresis behavior of the mean Nusselt number variation with Rayleigh number for $G = 0.200$ and $Pr = 0.706$.

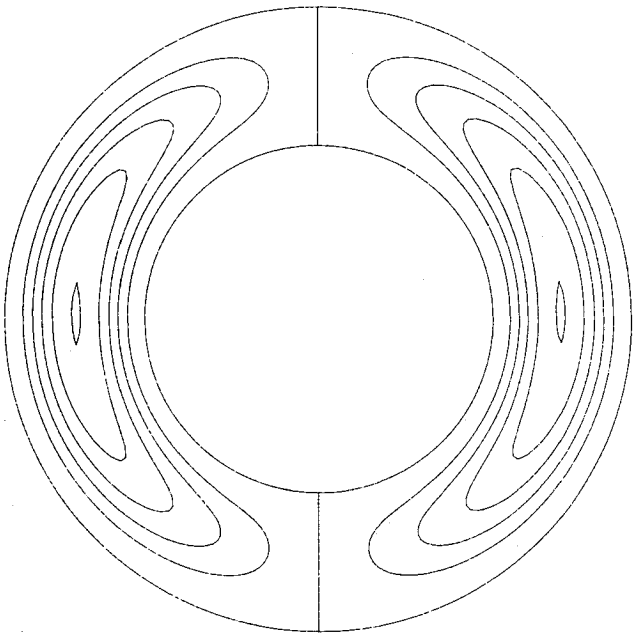

Fig. 3 Streamlines of a two-cellular flowfield at $Ra = 3.5 \times 10^5$ for $G = 0.200$ and $Pr = 0.706$.

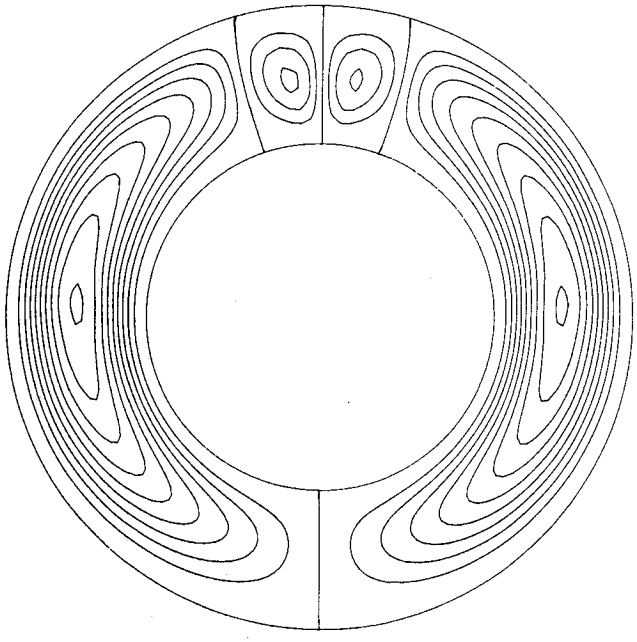

Fig. 4 Streamlines of a strong four-cellular flowfield at $Ra = 9 \times 10^5$ for $G = 0.200$ and $Pr = 0.706$.

Figure 4 shows the secondary flow in a strong state beyond transition at $Ra = 9 \times 10^5$. A typical multicellular temperature profile is also given in Fig. 5 for $Ra = 9 \times 10^5$. The shape of the isotherms was responsive to the fluid motion for $Pr = 0.706$, resulting in an inverted thermal plume near the top portion of the annulus.

Similarly, for $G = 0.100$, an abrupt rise in heat transfer occurred as the flowfield made the transition from two to six cells at $Ra = 2.841 \times 10^6$, as shown in Fig. 6. The hysteresis loop for this case expanded from $Ra = 2.57 \times 10^6$ to 2.84×10^6, a change of approximately 2.7×10^5. Below this range, only the two-cell solution prevailed, whereas above this range, only the six-cell solution prevailed.

The occurrence of six cells on transition may be explained as follows. As the gap decreases, curvature effects diminish,

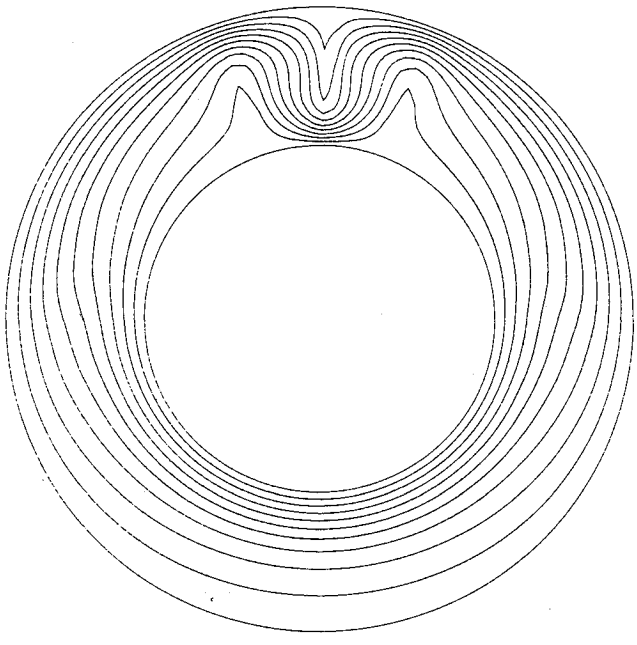

Fig. 5 Isotherms of the four-cellular flowfield at $Ra = 9 \times 10^5$ for $G = 0.200$ and $Pr = 0.706$.

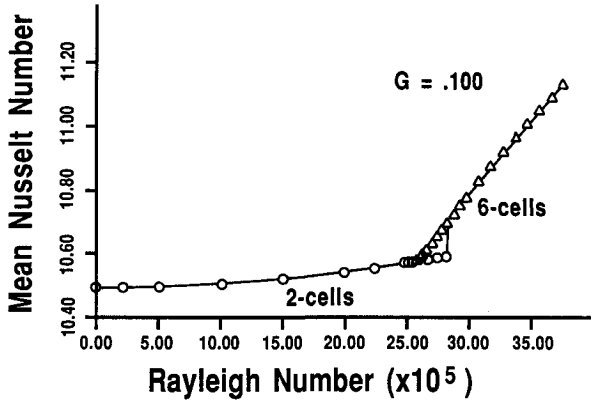

Fig. 6 Hysteresis behavior of the mean Nusselt number variation with Rayleigh number for $G = 0.100$ and $Pr = 0.706$.

resulting in a better comparison to the Benard type of instability between horizontal parallel flat plates. This, coupled with increased viscous effects, may cause the number of cells at transition to increase, i.e., a two- to six-cell transition for $G = 0.100$ as opposed to the two- to four-cell transition for $G = 0.200$. This statement is supported by the numerical results of Rao et al.,[8] where they graphically depicted a six-cell flow pattern at a Rayleigh number of approximately 7.5×10^5 for $G = 0.175$. In this study, for $G = 0.175$, a transition to six cells took place at $Ra = 4.5 \times 10^5$. A typical six-cell flow pattern with related isotherms for $G = 0.100$ and $Ra = 3.6 \times 10^6$ is depicted in Figs. 7 and 8, respectively. Notice the upright thermal plume (Fig. 8) associated with the six-cell flowfield.

A mesh resolution comparison given in Fant[9] indicates that the transitional Ra for $G = 0.200$ is within 15% uncertainty, whereas for the smaller gap $G = 0.100$, only a 5% uncertainty was predicted.

The three-term expression for vorticity in Eq. (25) was used to generate comparative data for the pretransitional two-dimensional Navier-Stokes numerical results. Comparisons of the inner-wall ($r = 0$) vorticity are given in Fig. 9.

Figure 9 displays the angular variation of the inner-wall vorticity for $\bar{G} = 4.0$ and $Pr = 0.706$. For $G = 0.200, 0.100,$

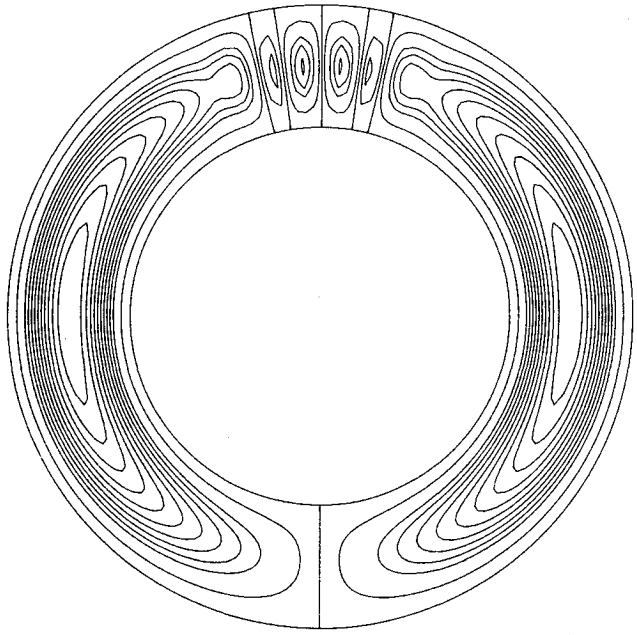

Fig. 7 Streamlines of a six-cellular flowfield at $Ra = 3.6 \times 10^6$ for $G = 0.100$ and $Pr = 0.706$.

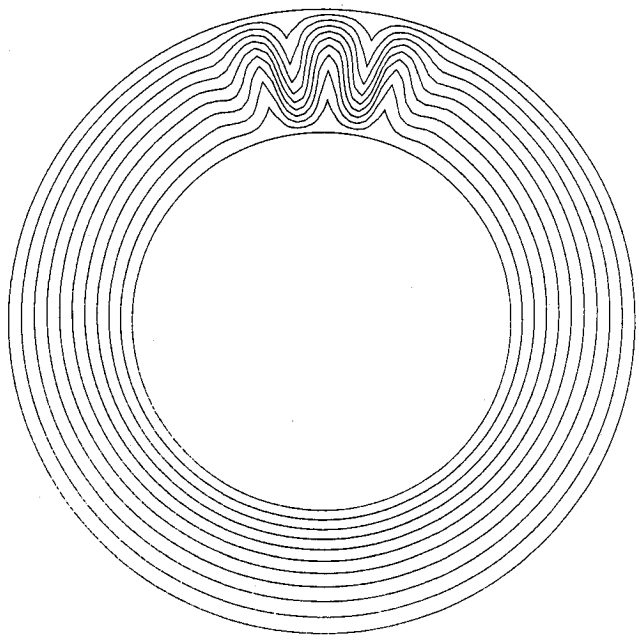

Fig. 8 Isotherms of the six-cellular flowfield at $Ra = 3.6 \times 10^6$ for $G = 0.100$ and $Pr = 0.706$.

and 0.025, maximum respective errors of 7.1, 3.5, and 1.0% resulted near $\psi = 90$ deg, or approximately the point of maximum fluid velocity.

The best comparison to the analytical result corresponded to $G = 0.025$. This was expected since the asymptotic analysis was tailored for the small gap/high Rayleigh number flow regime. Therefore, the two-dimensional Navier-Stokes solutions do indeed converge to the perturbation solutions as $G \rightarrow 0$.

Hydrodynamic Instability

Under certain conditions, an unsteady multicellular flow originates in the vertical sections of a two-dimensional narrow horizontal cylindrical annulus. This particular type of multicellular flow was captured numerically by solving the small Prandtl number Navier-Stokes equations, as previously derived. The multicells develop as a result of hydrodynamic instability and are analogous to those investigated by other researchers with regard to the vertical slot geometry (see Lee and Korpela[13]).

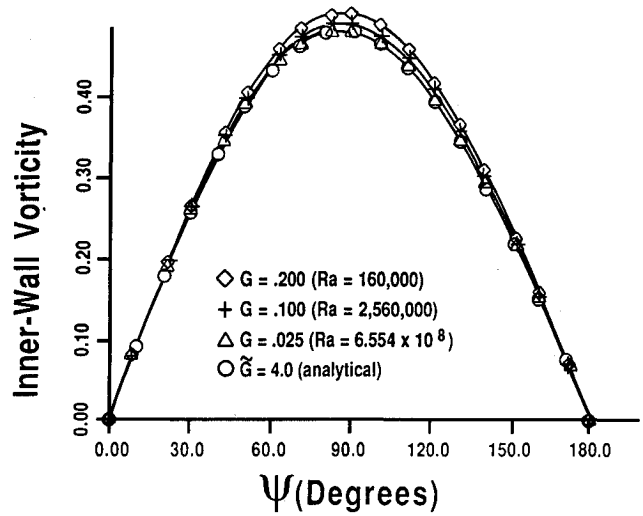

Fig. 9 Angular variation of the inner-wall vorticity for $\tilde{G} = Ra^{1/4} G = 4.0$, and $Pr = 0.706$.

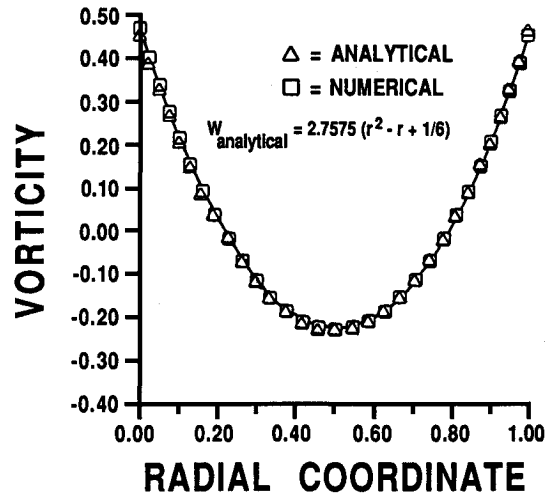

Fig. 10 Radial variation of vorticity at $\psi = 90$ deg for $G = 0.09$ and $Gr = 14.1 \times 10^6$.

For $G = 0.09$, steady-state unicellular results in the half annulus were obtained up to a Grashof number of 14.1×10^6. Figure 10 provides a comparison between numerical and analytical results for the radial variation of vorticity at $\psi = 90$ deg. The analytical vorticity expression used in Fig. 10 was obtained from the leading-order term of Eq. (35), with $\hat{G} = Gr^{1/4} G = 5.515$ (for $G = 0.09$ and $Gr = 14.1 \times 10^6$). These results indicate a maximum relative error of about 2.0% occurring at the inner and outer walls of the annulus. This favorable comparison again supports the numerical and analytical analyses used in this research.

At $Gr = 14.5 \times 10^6$, the $G = 0.09$ geometry initially developed a five-cell instability near the vertical portion of the annulus, as indicated by Fig. 11. This multicellular flow became unsteady and vacillated between four and five cells within the annulus, producing the time-periodic response of Fig. 12.

The period of this cyclic pattern is approximately 0.135 time units. This result is similar to that reported by Fant et al.,[14] where they resolved unsteady multicellular flow obtained by solving small Prandtl number boundary-layer equations.

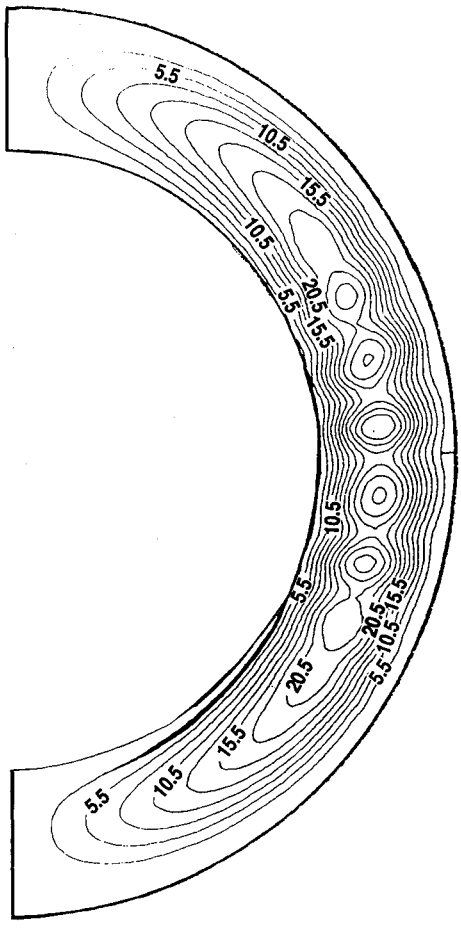

Fig. 11 Streamlines of a five-cellular flowfield for $G = 0.09$, $Gr = 14.5 \times 10^6$, and $t = 0.75$.

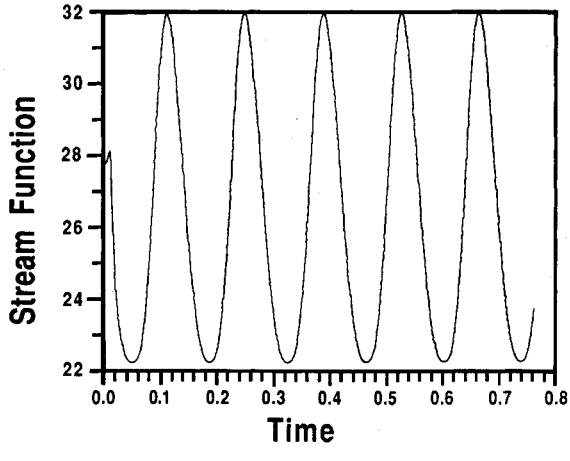

Fig. 12 Time dependence of the stream function at $r = 0.5$, $\psi = 90$ deg for $G = 0.09$, and $Gr = 14.5 \times 10^6$.

Finer meshes of 31 × 132 and 31 × 162 were also considered for this gap width. The transitional Grashof numbers for these meshes were 14×10^6 and 13.8×10^6, respectively. In addition, each mesh size resolved the same number of initial cells (five) at nearly the same location in the annulus.

Using the 31 × 102 mesh, transitional Grashof numbers for other size gap widths were calculated. These results plot as a straight line in Fig. 13. The slope of this line is −0.30, indicating that the gap spacing G for transition is proportional to $Gr^{-0.30}$. Apparently, this curve implies that the product

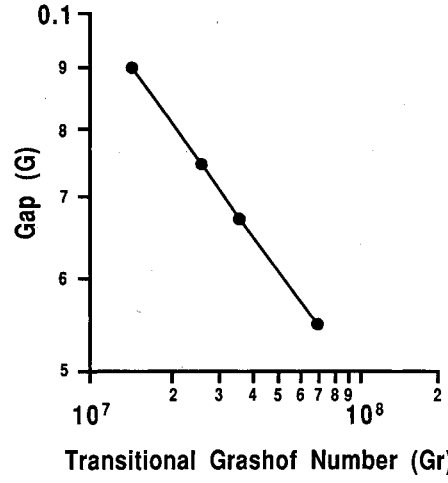

Fig. 13 Gap spacing as a function of transitional Grashof number.

$G \cdot Gr^{0.30}$ is equal to a constant at transition for small Prandtl number fluids. It was also noticed that the number of cells at transition increased as the gap width decreased.

This scaling is slightly different than that predicted by Fant et al.,[14] where they reported the gap to scale as $G \sim Gr^{-0.25}$ for small Pr boundary-layer equations. Note that in both studies the resulting multicellular flowfields were qualitatively similar.

Concluding Remarks

Numerical solutions of the two-dimensional Navier-Stokes equations yielded steady laminar multicellular flow for air near the top portions of narrow horizontal isothermal concentric cylinders. It was shown that hysteresis behavior exists for $G = 0.100$ and 0.200, with respect to sudden changes in the mean Nusselt number as the Rayleigh number was slowly increased and then decreased past the multicellular transition point. Pretransitional numerical results compared favorably to an existing analytical solution that was valid for high Rayleigh numbers and small gap widths.

Simplified equations for small Prandtl number were obtained from the two-dimensional Navier-Stokes equations. These equations were valid for arbitrary gap size and Grashof number and incorporated both radial and azimuthal diffusion terms in the vorticity equation. For various size small gap widths, numerical results demonstrated (at least qualitatively) that multicellular flow can indeed exist in the vertical portions of narrow annuli. In particular, an unsteady time-periodic multicellular instability was evident for $G = 0.09$ at $Gr = 14.5 \times 10^6$.

Based on these results and the work presented in Fant et al.,[14] an experimental verification of this small Prandtl number phenomenon is in order for this geometry.

Acknowledgments

D. B. Fant would like to acknowledge the support obtained from the United States Air Force for his research at the Air Force Institute of Technology and for the preparation of this manuscript. Also, partial support from the National Science Foundation Presidential Young Investigator Awards of J. Prusa and A. Rothmayer is recognized.

References

[1]Tsui, Y. T., and Tremblay, B., "On Transient Natural Convection Heat Transfer in the Annulus Between Concentric Horizontal Cylinders with Isothermal Surfaces," *International Journal of Heat and*

Mass Transfer, Vol. 27, 1984, pp. 103–111.

[2]Powe, R. E., Carley, C. T., and Bishop, E. H., "Free Convective Flow Patterns in Cylindrical Annuli," *Journal of Heat Transfer*, Vol. 91, 1969, pp. 310–314.

[3]Liu, C. Y., Mueller, W. K., and Landis, F., "Natural Convection Heat Transfer in Long Horizontal Cylindrical Annuli," *International Heat Transfer Conference*, 1961-62, pp. 976–984.

[4]Grigull, U., and Hauf, W., "Natural Convection in Horizontal Cylindrical Annuli," *International Fluids and Heat Transfer Conference*, Vol. 2, 1966, pp. 182–195.

[5]Bishop, E. H., Carley, C. T., and Powe, R. E., "Natural Convective Oscillatory Flow in Cylindrical Annuli," *International Journal of Heat and Mass Transfer*, Vol. 11, 1968, pp. 1741–1752.

[6]Powe, R. E., Carley, C. T., and Carruth, S. L., "A Numerical Solution for Natural Convection in Cylindrical Annuli," *Journal of Heat Transfer*, Vol. 93, 1971, pp. 210–220.

[7]Kuehn, T. H., and Goldstein, R. J., "An Experimental and Theoretical Study of Natural Convection in the Annulus Between Horizontal Concentric Cylinders," *Journal of Fluid Mechanics*, Vol. 74, 1976, pp. 695–719.

[8]Rao, Y. F., Miki, Y., Fukuda, K., Takata, Y., and Hasegawa, S., "Flow Patterns of Natural Convection in Horizontal Cylindrical Annuli," *International Journal of Heat and Mass Transfer*, Vol. 28, 1985, pp. 705–714.

[9]Fant, D. B., "The Numerical and Analytical Study of Bifurcation and Multicellular Flow Instability due to Natural Convection Between Narrow Horizontal Isothermal Cylindrical Annuli at High Rayleigh Numbers," *Ph.D. Dissertation*, Iowa State University, Ames, IA, August, 1987.

[10]Mack, L. R., and Bishop, E. H., "Natural Convection Between Horizontal Concentric Cylinders for Low Rayleigh Numbers," *Quarterly Journal of Mechanics and Applied Mathematics*, Vol. 21, 1968, pp. 223–241.

[11]Huetz, J., and Petit, J. P., "Natural and Mixed Convection in Concentric Annular Spaces—Experimental and Theoretical Results for Liquid Metals," *Proceedings of the Fifth International Heat Transfer Conference*, Tokyo, Japan, 1974.

[12]Elder, J. W., "Laminar Free Convection in a Vertical Slot," *Journal of Fluid Mechanics*, Vol. 23, 1965, pp. 77–98.

[13]Lee, Y., and Korpela, S. A., "Multicellular Natural Convection in a Vertical Slot," *Journal of Fluid Mechanics*, Vol. 126, 1983, pp. 91–121.

[14]Fant, D. B., Prusa, J., and Rothmayer, A. P., "Unsteady Multicellular Natural Convection in a Narrow Horizontal Cylindrical Annulus," *AIAA First National Fluid Dynamics Congress*, Cincinnati, OH, July, 1988, pp. 1922–1934.

[15]Prusa, J., and Yao, L. S., "Natural Convection Heat Transfer Between Eccentric Horizontal Cylinders," *Journal of Heat Transfer*, Vol. 105, 1983, pp. 108–116.

[16]Bishop, E. H., Kolflat, R. S., Mack, L. R., and Scanlan, J. A., "Convective Heat Transfer Between Concentric Spheres," *Proceedings of Heat Transfer and Mechanics*, 1964, pp. 69–80.